ELSEVIER

Materials Science and Engineering A 452–453 (2007) 773–780

MATERIALS SCIENCE & ENGINEERING A

www.elsevier.com/locate/msea

Mechanical properties of partially sintered materials

Yuttanant Boonyongmaneerat *,[1]

Department of Materials Science and Engineering, Massachusetts Institute of Technology, Cambridge, MA 02139, United States

Received 8 June 2006; received in revised form 26 October 2006; accepted 3 November 2006

Abstract

In powder materials that are sintered only in the initial stage, a continuous network of pores remains in the structure. Here the mechanical properties of partially sintered materials are investigated in relation to processing parameters, sintering behavior, and microstructure, using, as a model material, W prepared by the activated sintering technique at low firing temperatures. Hardness and fracture toughness of partially sintered W are found to be critically dependent on the interparticle neck size of W sintered particles, which is in turn affected by the sintering additives. While fracture toughness is apparently solely a function of densification and interparticle neck size, hardness scales with a factor that combines both sintered density and densification. Existing analytical models for these scaling behaviors are compared critically with the new data.

Keywords: Hardness; Fracture toughness; Partially sintered; Activated sintering; Tungsten

1. Introduction

The process of sintering allows near-net shape manufacturing of components at temperatures below their melting points, and consequently has been widely employed in numerous applications [1,2]. The sintering process is generally described by three sequential stages called the initial, intermediate and final stages of sintering. In the initial stage, necks grow between sintered particles, and the degree of shrinkage and densification is relatively low. At higher sintered density, generally above 80% TD (theoretical density), the formation of interconnected pores and pore isolation occur, marking the intermediate and final stages, respectively. Sintering protocols, namely firing time and temperature, are among the factors that control the progression through these stages.

It is clear that in many applications it is desirable to sinter powder materials through all three stages to full density, such that optimum strength is achieved. In some applications, however, full sintering is not required or may even be undesirable from the point of view of property control or economics. For example, a sintered ceramic shell used in investment casting needs to contain some porosity, so that steams can be transferred through the mold during the autoclave operation and so that entrapped gas can migrate out of the mold during the metal casting step [3,4]. Anode substrates for solid oxide fuel cells can be processed by tape casting and sintering, and require a high residual porosity level so that fuel can reach the electrolyte interface [5–7]. Finally, melt–infiltration processes for fabrication of metal matrix composites require a partially sintered porous preform with fully open porosity [8]. A continuous network of pores is present in all of theses cases, and the mechanical properties of the component rely on the transmission of stress across interparticle necks of the partially sintered powder particles.

While a large number of publications have concentrated on the mechanical response of highly densified sintered materials [9–16], fundamental studies on the mechanical properties of those with low sintered density (i.e., sintered only in the initial stage) are much more limited [17–20]. It is the purpose of this paper to examine the mechanical properties of partially sintered materials, particularly hardness and fracture toughness, and to clarify the relationships between material properties, sintering parameters, and microstructure. Our study is performed on a single system, namely tungsten (W) containing minority additions of sintering activators.

2. Analytical

Arato et al. were one of the first groups to consider the mechanical properties of partially sintered materials in rela-

* Present Address: Department of Materials Science and Engineering, Northwestern University, Evanston, IL 60208, United States. Tel.: +1 847 467 5416; fax: +1 847 491 7820.

E-mail address: vee@alum.mit.edu.

[1] The author will assume a research position at the Metallurgy and Materials Science Research Institute, Chulalongkorn University, Thailand, in 2007.

0921-5093/$ – see front matter © 2006 Elsevier B.V. All rights reserved.
doi:10.1016/j.msea.2006.11.043

tion to their microstructure [17]. They derived an analytical scaling relationship for elastic modulus through the determination of forces acting across particle contacts and on a reference plane through the structure, using a Voigt average for the elastic properties of a polycrystalline body. The resulting expression for Young's modulus is nominally valid for the initial stage of sintering [21]:

$$E = E_0 \frac{z}{4} \rho_s \left(\frac{r}{R}\right)^2 \quad (1)$$

Here E and E_0 are the Young's moduli of partially sintered and fully dense material, respectively, z is the average coordination number of the sintering particles of mean radius R, ρ_s is the fractional sintered density (relative density), and r is the interparticle neck radius. The dimensionless ratio r/R will be termed the "relative neck radius". Arato et al. further suggested that the hardness of a partially sintered compact, H, would scale similarly

$$H = \frac{E}{E_0} H_0 \quad (2)$$

where H_0 is hardness of the fully dense material. The general scaling of Eq. (2) has been experimentally validated by Luo and Stevens [19], who measured the bulk modulus and hardness of stabilized zirconia sintered to densities $\rho_s = 0.6$–1.0. Combining Eqs. (1) and (2), the hardness of partially sintered material may also be written as

$$H = \left(\frac{z}{4} \rho_s \left(\frac{r}{R}\right)^2\right) H_0 \quad (3)$$

Eqs. (1) and (3) give simple scaling relationships for modulus and hardness with respect to the density of a partially sintered compact. However, the microstructural state variables z and r/R also evolve with sintered density, and must be modeled to reduce the above expressions to simple functions of ρ_s. For example, Arato et al. used Fischmeister and Arzt's model [22,23] for the densification of an irregular packing of spherical particles to capture the evolution of z and r/R as a function of the sintering profile (density), and compared the resulting model with hardness measurements performed on Si_3N_4-based sintered compacts having sintered density in the range $\rho_s = 0.6$–0.9. The results from the experiments were found to be in good agreement with the predictions of Eqs. (1) and (3).

In addition to their discussion of hardness, Arato et al. also modeled the fracture toughness, K_{IC}, of partially sintered brittle materials using Griffith's fracture theory:

$$K_{IC} = \sigma_0 R^{1/2} \frac{E}{E_0} = \sigma_0 R^{1/2} \left(\frac{z}{4} \rho_s \left(\frac{r}{R}\right)^2\right) \quad (4)$$

In Eq. (4), σ_0 is the tensile strength of flaw-free fully dense material. Fracture toughness was also considered later by Green and Hardy [18], who derived a different theoretical model for partially sintered brittle materials by modifying existing models for fracture toughness of cellular ceramics [24]. With the assumption that partially sintered particles fail by a crack passing through sintered interparticle contacts (i.e., necks) and that one contact is broken at a time, the authors argued that tensile stress, σ, acting on an unbroken neck ahead of a crack is responsible for fracture of the material, and is given by

$$\sigma = \left(\frac{2}{\pi}\right)^{1/2} \left(\frac{K_I}{\pi r^2}\right) (2R)^{3/2} \quad (5)$$

where K_I is the stress intensity factor in mode I loading. As σ is increased and reaches the intrinsic strength of the neck, σ_0, fracture occurs, and the critical stress intensity is written as

$$K_{IC} = C_0 \sigma_0 R^{1/2} \left(\frac{r}{R}\right)^2 \quad (6)$$

where $C_0 \approx 1.4$ is a numerical constant.

Unlike Arato et al.'s model (Eq. (4)), Green and Hardy's solution in Eq. (6) does not contain an explicit sintered density dependency, and, as before, a microstructural model is required to link r/R to ρ_s. However, neither of these two models has been rigorously tested against experimental data. Green and Hardy did examine the fracture toughness of sintered alumina over a relatively narrow range 58–64% TD, and found reasonable agreement with the form of Eq. (6). However, in the narrow range of sintered densities they investigated, their model (Eq. (6)) and Arato et al.'s (Eq. (4)) give very similar predictions.

Despite the differences among the various analytical models described above, they all contain an explicit dependence on the relative neck radius. This highlights the importance of neck formation on the evolution of strength in the initial stage of sintering. Several expressions for the relationship between the relative neck radius, r/R, and sintered density, ρ_s, have been proposed, some of which are shown in Table 1 and plotted as a function of sintered density, for the case of sintered materials with green density $\rho_g = 0.5$ and 0.64, in Fig. 1 [22,23,25,26]. As shown in the figure, all four models suggest a monotonic increase of relative neck radius with sintered density. In the initial stage of sintering of concern to this work ($0.5 < \rho_s < 0.75$), the predicted r/R is significantly different from one model to another. In the later stages of sintering, these differences become even more pronounced; compared to the expected limit $r/R \to 1$ as $\rho_s \to 1$, the relationships of Fischmeister and Arzt [22,23] and Helle et al. [26] underestimate the relative interparticle neck radius, while Skorokhod's initial stage model [25] overestimates it.

Table 1
Proposed relationships between the relative interparticle neck radius and densities

Fischmeister and Arzt [22,23]	$\left(\frac{r}{R}\right)^2 = 1.75(\rho_s - \rho_g)(1 - (\rho_s - \rho_g))$
Skorokhod (initial stage) [25]	$\left(\frac{r}{R}\right)^2 = \frac{4}{3} \ln\left(\frac{1-\rho_g}{1-\rho_s}\right)$
Skorokhod (all stages) [25]	$\left(\frac{r}{R}\right)^2 = 1 - \left(\frac{1-\rho_s}{1-\rho_g}\right)^{4/3}$
Helle et al. [26]	$\left(\frac{r}{R}\right)^2 = \frac{1}{3}\left(1 - \left(\frac{1-\rho_s}{1-\rho_g}\right)\right)$

Most of the relationships presented in Table 1 can be explicitly expressed in terms of *densification*, $\tilde{\rho}$—a sintering parameter that is defined as the relative change of density with respect to

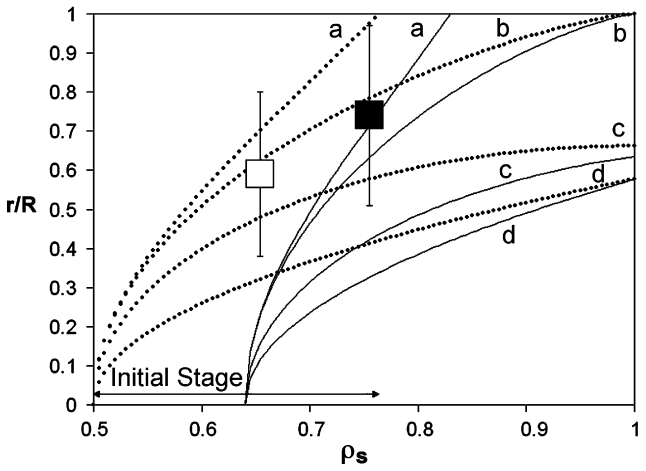

Fig. 1. The relative neck radius of powders with green density, ρ_g of 0.5 (···) and 0.64 (–) as a function of sintered density, ρ_s, according to the models of (a) Skorokhod (initial stage) [25], (b) Skorokhod (all stages) [25], (c) Fischmeister and Arzt [22,23], and Helle et al. [26] (see Table 1). Also shown on the plot are the average values of relative neck radius of (i) series A sintered powders with $\rho_g = 0.5$ and $\rho_s = 0.65$ (□), and (ii) series B sintered powders with $\rho_g = 0.64$ and $\rho_s = 0.76$ (■).

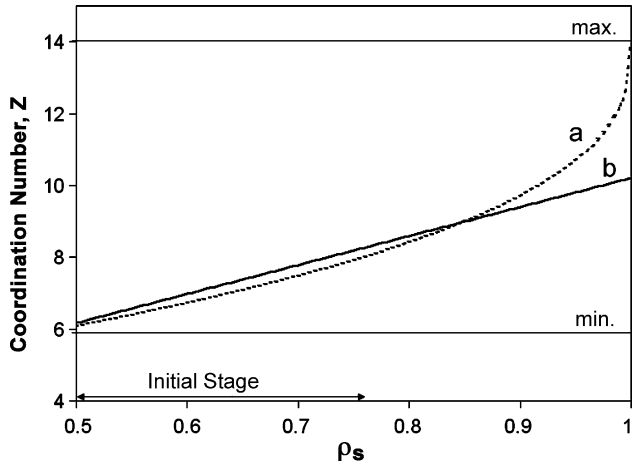

Fig. 2. The coordination number of powders as a function of sintered density, ρ_s, according to the models of (a) German [28] and (b) Fischmeister and Arzt [22,23] (see Table 2). The highest and lowest values of the coordination number possible are 6 and 14, respectively, as shown on the plot.

the green density, ρ_g (i.e., compact density), according to

$$\tilde{\rho} = \frac{\rho_s - \rho_g}{1 - \rho_g} \tag{7}$$

For example, Skorokhod's model may be written as

$$\left(\frac{r}{R}\right)^2 = 1 - \left(\frac{1-\rho_g}{1-\rho_s}\right)^{4/3} = 1 - (1-\tilde{\rho})^{4/3} \tag{8}$$

This signifies that densification, $\tilde{\rho}$, may be regarded as a sintering parameter that describes the relative interparticle neck radius of sintered materials. Two sets of sintered materials can be sintered to very different levels of sintered density, but to the same *densification* (and hence the same relative neck radius), provided they have different green densities.

Another variable that enters into Eqs. (1), (3) and (4), is the average coordination number of sintered particles, z, which increases as the structure forms new contacts upon sintering. Several models have been proposed for z as a function of sintered density [22,23,27,28]; two such models are presented in Table 2 and Fig. 2. Due to geometric constraints, the minimum and maximum coordination number that mono-sized spherical particles can exhibit is 6 and 14, respectively. Unlike r/R, the values of z as predicted by different models do not differ from one another significantly in the lower range of sintered density relevant to initial stage sintering ($0.5 < \rho_s < 0.75$).

To briefly summarize, various models have been proposed to describe the relationship between the structure and mechanical properties of partially sintered materials. However, some such models exhibit fundamentally distinct scaling from one another, even for the same predicted property. Furthermore, experimental works performed to justify these models are very limited, and not conclusive. Here we present an experimental study aimed at a quantitative evaluation of both the hardness model proposed by Arato et al. and the fracture toughness models proposed by Arato et al. and Green and Hardy. The investigation is performed on partially sintered W containing minority additions of sintering activators, and with a broad range of sintered density as well as densification. Similar to the situation for other sintered material systems, studies of the mechanical properties of partially sintered W are very limited [29].

Table 2
Proposed relationships between coordination number of sintered particles and relative density

Fischmeister and Arzt [22,23]	$z = 7.3 + 8.07(\rho_s - 0.64)$
German [28]	$z = 14 - 10.3(1-\rho_s)^{0.38}$

3. Experimental procedure

W powder was chosen for the present study for several main reasons. First, W is used in a variety of refractory applications [30,31], and due to its very high melting point of 3410 °C, W is primarily formed into desirable shapes by powder processing. Typical firing temperatures for W are above 2700 °C to achieve high sintered density [30,32]. Second, the sintering kinetics of W particles can be dramatically enhanced by the addition of very small quantities of transition metals such as Ni, Fe and Pd, through the process of activated sintering [33,34], and this allows W to be sintered at lower temperatures. Here, we use this approach to control density and densification of sintered W. Finally, it is known that W fractures in a brittle mode at room temperature [35], a necessary condition to test Eqs. (4) and (6).

Two series of W powders, which we will label series A and B, were used in this study (see Table 3 for some characteristics of these powders). These powders were manufactured by GE Lighting Components (Cleveland, OH) and Alldyne Powder Technologies (Huntsville, AL), respectively, and had mean particle sizes of 1.2 μm (A) and 1.7 μm (B). Due to the different particle size distributions of the two powders, as shown in Fig. 3, the tap densities of powders A and B were quite different (see Table 3). In order to manipulate the sintering properties of these

Table 3
The characteristics of W powders in series A and B

Property	A	B
Mean size (μm)	1.2	1.7
Tap density (% TD)	42	60
Compact density (% TD)	50	64
Ni impurity (wt.%)	<0.0005	0.006
Fe impurity (wt.%)	<0.001	0.018

powders, various minority additions of Ni (2.2–3 μm) and Fe (1–3 μm) powders were added to the W powder by dry mixing following the general procedure of Ref. [36]. It should be noted that a small initial content of sintering activators (Ni and Fe) was also present as impurities, particularly in powder B (Table 3).

After dry mixing, green compact specimens were made using a single-action cold press and a stainless-steel die of rectangular cross section, a geometry chosen to facilitate measurement of fracture toughness. A compaction pressure of 21 MPa was employed, resulting in compact densities of 50 and 64% TD in series A and series B specimens, respectively. These green specimens were then sintered in a furnace programmed with a heating rate of 5 °C/min and an isothermal hold at 1177 °C for 1 h, followed by slow furnace cooling. To prevent the oxidation of W, the processing was carried out in a dry 3% H_2–97% N_2 atmosphere. The geometry of the fired specimens was approximately 24 mm × 8 mm × 3 mm.

Sintering properties including linear shrinkage ($\Delta L/L_0$), sintered density (ρ_s) and densification ($\tilde{\rho}$) were determined from the measured dimensions of the as-fired specimens. As will be discussed in more detail later, the two chosen series of W powders with processing parameters as described resulted in specimens with a broad range of sintered density and densification in the initial stage, ranging over $\rho_s = 0.51$–0.75, and $\tilde{\rho} = 0.03$–0.31, respectively. Hardness measurements were performed using a Vickers micro-indenter with a load of 100 g. To measure fracture toughness, the single-edge notched three point bending test [37,38] was conducted on test specimens containing a notch cut by a diamond knife with an approximate depth of 1 mm. For every mechanical property reported, at least two identical specimens were prepared and tested. In the case of hardness, the reported values are the averages of at least four measurements.

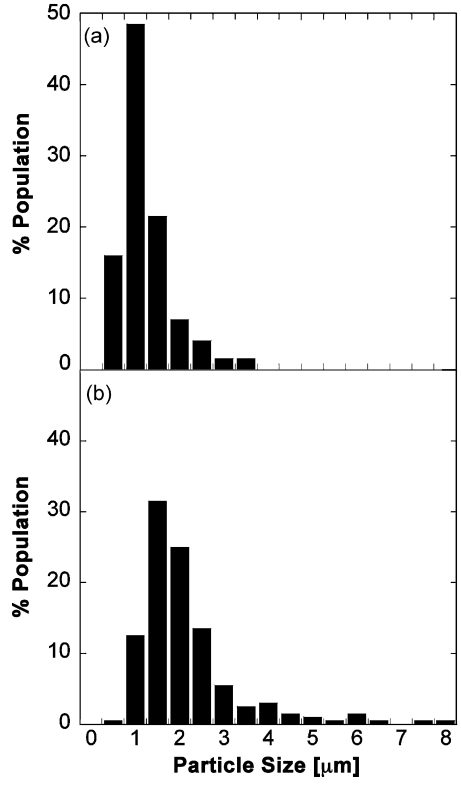

Fig. 3. Particle size distribution of (a) 'series A' and (b) 'series B' tungsten powders.

4. Results

The linear shrinkage of series A and B specimens after sintering is shown in Fig. 4. In both series, the maximum shrinkage is observed for the highest content of Ni additive (0.18 and 0.10 wt.%. for series A and B, respectively). When the same amount of Fe was added to powder A, significantly less sintering shrinkage was observed. This result suggests that Ni improves the sintering kinetics of W much more than does Fe, in agreement with prior observations [33]. In the range of low density of concern here, sintering shrinkage relates linearly to sintered density. Due to their relatively higher green density, series-B specimens exhibited higher sintered densities even while they experienced a very small degree of shrinkage. The results in Fig. 4 also suggest that the correlation of shrinkage and sintered density is independent of the particular activators added, as the various points collected there correspond to specimens with Ni, Fe and Ni + Fe additions.

Fig. 5a–d presents the microstructure of fired specimens prepared with powders A and B which experienced the smallest (a and c) and largest (b and d) sintering shrinkage. The micrographs clearly show that with increasing content of sintering activators,

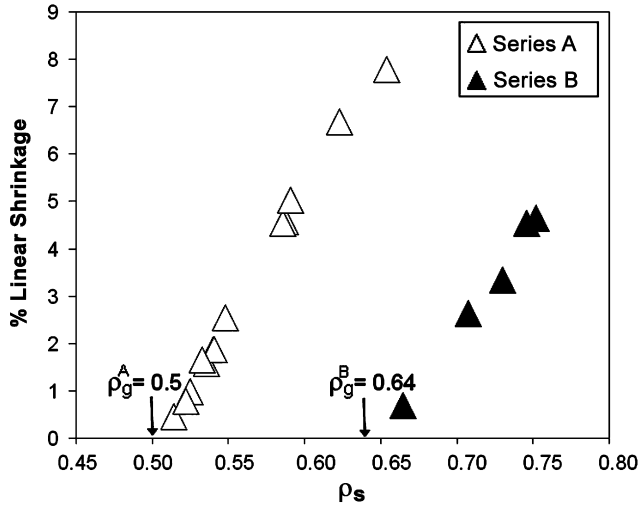

Fig. 4. The percent linear shrinkage of W compacts prepared with series A and B powders containing various contents of sintering additives. The shrinkage is presented as a function of sintered density.

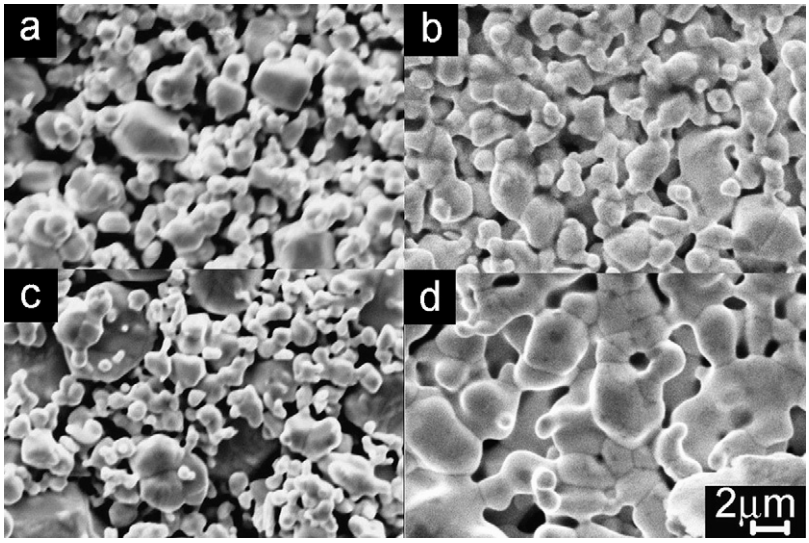

Fig. 5. SEM micrographs of W compacts prepared with (a) series A powder ($\rho_s = 0.51$), (b) series A powder containing 0.18 wt.% Ni ($\rho_s = 0.65$), (c) series B powder ($\rho_s = 0.67$), and (d) series B powder containing 0.10 wt.% Ni and 0.02 wt.% Fe ($\rho_s = 0.75$). The specimens shown in (b) and (d) contained the highest amounts of additives used to prepare series A and B specimens, respectively.

the bonding between W particles is promoted. At the maximum content of sintering activators employed, irregular pore shapes can still be observed in both series of specimens, indicating that sintering remains in the initial stage.

The hardness and fracture toughness of the specimens as a function of the sintering activator concentration are respectively shown in Fig. 6a and b, using for the latter quantity the monolayer coverage of activators, $\overline{M}$, on the surface of W powders. This parameter was calculated by integrating monolayer coverage over the particle size distributions, assuming spherical particles:

$$\overline{M} = \frac{\int P(r)(r/2a)[(1 + (c/1 - c)(\rho_w/\rho_a))^{1/3} - 1]\ \mathrm{d}r}{\int P(r)\ \mathrm{d}r} \quad (9)$$

where r is the particle radius of W, $P(r)$ is the number population of W powders at any particle size, c and a are the concentration and atomic radius of sintering activators, respectively, and ρ_w and ρ_a are the theoretical densities of W and additives.

With a slight increase of the sintering activator concentration (amounting to only a few monolayers), the hardness and fracture toughness of the specimens in both series increased considerably (Fig. 6a and b), and roughly in proportion to the sintered density (Fig. 7a and b). The exception to this observation is the specimens in series A that contained Fe, whose toughness slightly declined at relatively high Fe content. As shown in Fig. 7a and b the hardness and fracture toughness of the specimens was essentially zero at the green density, and increased monotonically with sintered density, even though different combinations of sintering activators were used. The results therefore suggest that hardness and fracture toughness are dominated by the evolution of the partially sintered microstructures of the specimens, which is in turn influenced by the sintering activators, Ni and Fe; the direct effect of a small concentration of the additives on hardness is not obviously significant.

The fracture surfaces of the specimens employed in the fracture test were analyzed in a scanning electron microscope, and

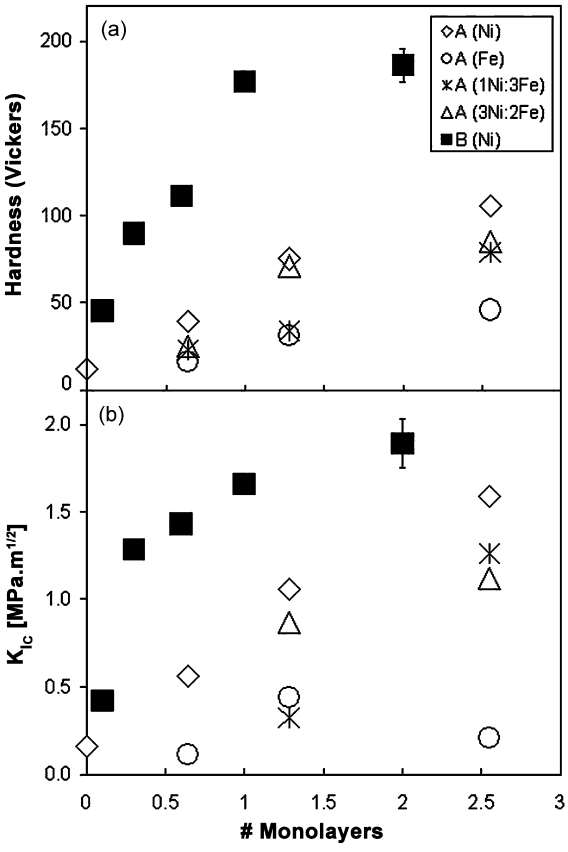

Fig. 6. The average (a) Vickers hardness and (b) fracture toughness of W compacts prepared with series A and B powders that contained various types and contents of sintering additives. The content of sintering activators is presented in terms of monolayer coverage of activators on the surface of W particles. A representative error bar is presented for one of the data sets on each curve to show the degree of deviation in the data obtained.

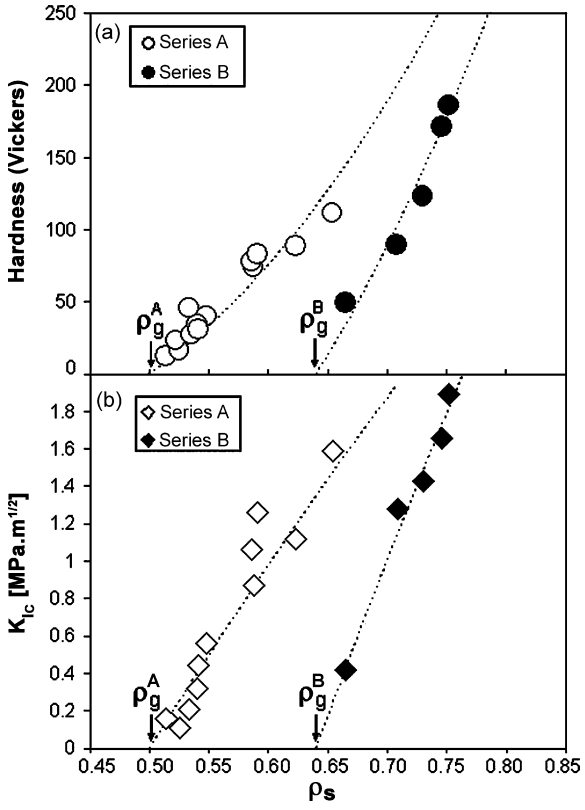

Fig. 7. The average (a) Vickers hardness and (b) fracture toughness of W compacts prepared with series A and B powders, as a function of sintered density. Trendlines are shown for visualization purposes only.

it was observed that the surfaces of particles across the fracture surface were smooth and no ductile dimples were apparent on the surfaces (not shown). This result suggests that fracture occurred along sintered contacts in a brittle fashion.

5. Discussion

It can be deduced from Fig. 7a and b that sintered density is a poor microstructural state variable with which to predict mechanical properties of partially sintered W, because this parameter alone does not account for the microstructural evolution that occurs upon sintering from different green densities. Consequently, different parameters are required to predict the properties of the material. In this section, the applicability of scaling factors for hardness and toughness, proposed in the various models described earlier will be examined.

To compare the Arato et al. and Green and Hardy models to our experimental data, some knowledge of z and r/R is essential. Since the values of the average coordination number, z, proposed in different models do not differ significantly from one another, as shown in Fig. 2, it is assumed here that z follows Fischmeister and Arzt's model. The models for r/R, on the other hand, are somewhat different from one another (Fig. 1). To justify a choice of model to be used here, the relative neck radius from two sets of specimens, one from each powder series, was measured. This was accomplished by measuring interparticle neck size and particle size of over 100 interparticle contacts from each set on scanning electron micrographs. Many local values of r/R were measured, and the average and standard deviation of the measurements are shown in Fig. 1. The relative neck radius of specimens from both experimental sets matches fairly well with that given in Skorokhod's "all-stage" model. Furthermore, Skorokhod's all-stage model is the only one which appropriately extrapolates to $r/R = 1$ at full density. For these reasons, Skorokhod's model was chosen for the comparisons that follow.

5.1. Hardness

A first attempt to normalize hardness for the effect of green density is shown in Fig. 8a, where the hardness of the specimens in series A and B is plotted as a function of densification. However, just as was observed in Fig. 7, two distinct curves can be discerned for series A and B, although they appropriately converge to a hardness of zero as densification decreases. Densification alone therefore does not explicitly predict the hardness of the material, and we therefore turn to a more complex normalization based on Arato et al.'s model (Eq. (3)).

Introducing Skorokhod's model for relative neck radius (Eq. (8)) into Arato et al.'s hardness model (Eq. (3)), we see that hardness is proportional to $z\rho_s(1-(1-\tilde{\rho})^{4/3})$. Our experimental

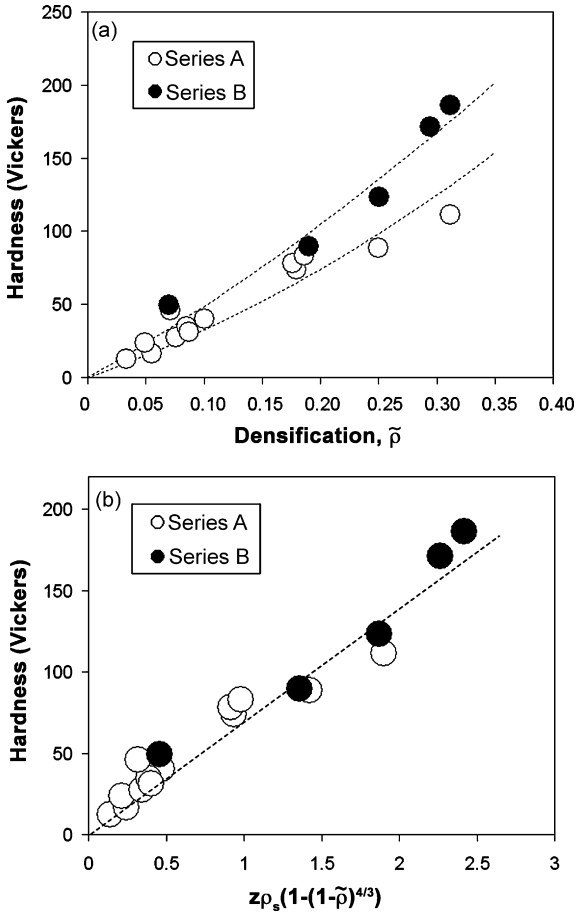

Fig. 8. Vickers hardness of W compacts in series A and B (a) as a function of densification, and (b) as a function of a factor which contains the coordination number (z), the sintered density (ρ_s), and densification ($\tilde{\rho}$). Trendlines are prescribed for visualization purposes.

data is plotted as a function of this scaling factor in Fig. 8b, where the two separable trends observed earlier for powders A and B in Figs. 7a and 8a collapse into a single, monotonic trend. This result signifies that hardness of partially sintered W cannot be predicted knowing either sintered density or densification alone, but is related to both sintering parameters; Arato et al.'s model reasonably captures the hardness evolution of the present partially sintered materials.

5.2. Fracture toughness

We first compare our data to Arato et al.'s model for fracture toughness [17]. Examining Eqs. (3) and (4), we observe that the scaling factor for fracture toughness proposed by Arato et al. has a similar form as that of hardness, with $K_{IC} \propto R^{1/2} z\rho_s(1-(1-\tilde{\rho})^{4/3})$. The fracture toughness of W normalized by $R^{1/2}$ is plotted as a function of this factor in Fig. 9a. Unfortunately, Arato et al.'s model neither convincingly linearizes our data nor collapses the two data series into a single trend. While the two trendlines start from the origin, they deviate from one another as the value on the x-axis increases.

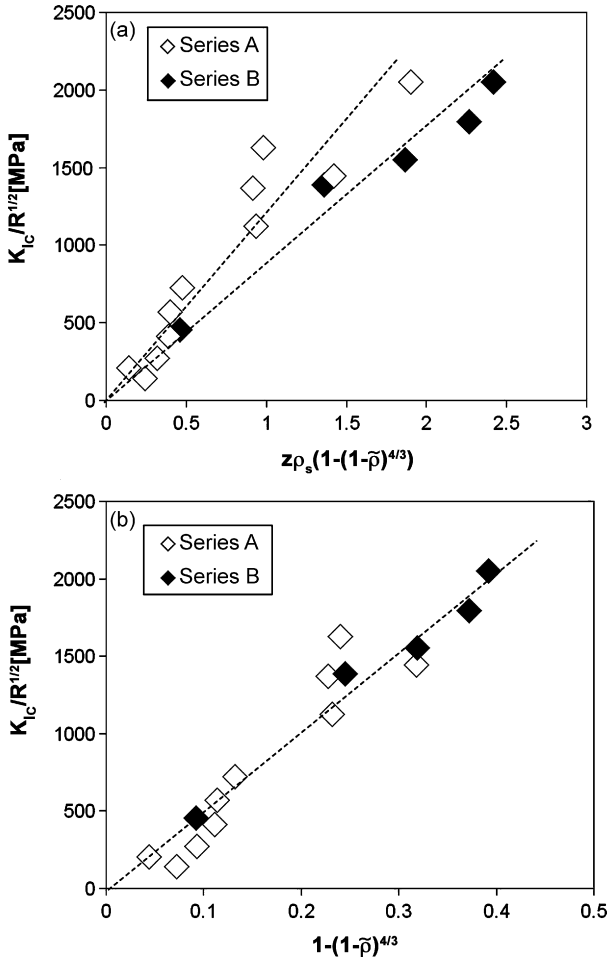

Fig. 9. Normalized fracture toughness of W compacts in series A and B (a) as a function of a factor which contains the coordination number (z), the sintered density (ρ_s), and densification ($\tilde{\rho}$), and (b) as a function of a factor which solely depends on densification. Trendlines are prescribed for visualization purposes.

To examine the applicability of Green and Hardy's fracture toughness model, which suggests a more explicit dependence of fracture toughness on interparticle neck size (Eq. (6)), we plot $K_{IC}/R^{1/2}$ as a function of $(1-(1-\tilde{\rho})^{4/3})$, which is equivalent to $(r/R)^2$ according to Eq. (8). The result presented in Fig. 9b exhibits data that are reasonably aligned in a single monotonic trend. The toughness extends to zero as interparticle neck size decreases to zero, as expected, and increases linearly with the increase of neck size, in agreement with Green and Hardy's model. This trend underscores the importance of interparticle neck size on fracture toughness and that fracture toughness is related to a scaling factor of $(r/R)^2$.

It should be noted that the factor $(1-(1-\tilde{\rho})^{4/3})$ may be written in terms of a Taylor expansion series with the first term being $(4/3)\tilde{\rho}$. Since this first term sufficiently describes the polynomial function at low values of densification ($\sim$<0.5), the fracture toughness of partially sintered materials may in many cases be adequately described using only the densification parameter and the mean particle size R. At high densification, on the other hand, the factor $(1-(1-\tilde{\rho})^{4/3})$ predicts that the fracture toughness of sintered materials will deviate from the linear trend. These findings are consistent with the experimental results obtained by Lam et al. [20] who investigated the fracture response of sintered alumina. In their investigation, the authors measured the fracture toughness of sintered alumina which had a mean particle size of 1 μm, densification within the range 0.16–0.94, and relative green density of 0.5 or 0.62. Their experiment reveals that fracture toughness is linearly related to the densification parameter for densification values up to ~0.4–0.6, all of which correspond to the initial-stage of sintering regime. Beyond those densification values, the fracture toughness of sintered alumina starts to deviate from the linear trend.

6. Conclusions

In the regime of low sintering activator content and low processing temperatures chosen for this study, activated W compacts were partially sintered and remained in the initial stage of sintering. The mechanical properties of W were improved with sintering enhancement, and the relationship between mechanical response and sintered density was found not obviously dependent to the type or content of sintering additives used. The mechanical properties of the partially sintered W compacts were critically controlled by relative interparticle neck size—a sintering property whose value can be estimated from the densification parameter. Specifically, hardness of partially sintered materials is explicitly related to both sintered density and densification, in accordance with Arato et al.'s hardness model. On the other hand, fracture toughness (normalized by a square root of particle radius) scales explicitly with densification but apparently not with sintered density, an effect captured by Green and Hardy's fracture toughness model for partially sintered materials.

Acknowledgements

The author would like to express his sincere gratitude to Prof. C.A. Schuh of Massachusetts Institute of Technology for

valuable discussions and guidance, and to the Metallurgy and Materials Science Research Institute, Chulalongkorn University, for their support.

References

[1] G. Petzow, W.A. Kaysser, J. Kunesch, Diffus. Defect. Data Solid State Data B 8/9 (1990) 3–36.
[2] A.S. Wronski, J. Mascarenhas, Mater. Sci. Forum 455/456 (2004) 253–257.
[3] S. Jones, C. Yuan, J. Mater. Process. Technol. 135 (2003) 258–265.
[4] S. Jones, M.R. Jolly, K. Lewis, Br. Ceram. Soc. Trans. 101 (2002) 106–113.
[5] B.P. Gorman, H.U. Anderson, J. Am. Ceram. Soc. 88 (2005) 1747–1753.
[6] H. Li, C. Xia, X. Fang, X. He, X. Wei, G. Meng, Key Eng. Mater. 280–283 (2005) 779–784.
[7] M. Boaro, J.M. Vohs, R.J. Gorte, J. Am. Ceram. Soc. 86 (2003) 395–400.
[8] H.X. Peng, Z. Fan, J. Evans, Mater. Sci. Technol. 16 (2000) 903–907.
[9] N.S. Stoloff, Mater. Sci. Eng. A 261 (1999) 169–180.
[10] G. Zielger, J. Mater. Sci. 22 (1987) 3041–3086.
[11] R. Vassen, J. Mater. Process. Technol. 92-93 (1999) 77–84.
[12] T.D. McGee, Mater. Sci. Res. (1965) 3–32.
[13] I.V. Nel'zina, I.D. Radomysel'skii, Sov. Powder Metall. Met. Ceram. 20 (1981) 854–862.
[14] K. Churn, R.M. German, Metall. Mater. Trans. 15A (1984) 331–338.
[15] A. Bose, R.M. German, Metall. Mater. Trans. 21A (1990) 1325–1327.
[16] O. Horacsek, L. Bartha, Phys. Sinter. 5 (1973) 85–94.
[17] P. Arato, E. Besenyei, A. Kele, F. Weber, J. Mater. Sci. 30 (1995) 1863–1871.
[18] D.J. Green, D. Hardy, J. Mater. Sci. Lett. 15 (1996) 1167–1168.
[19] J. Luo, R. Stevens, Ceram. Int. 25 (1999) 281–286.
[20] D.C.C. Lam, F.F. Lange, A.G. Evans, J. Am. Ceram. Soc. 77 (1994) 2113–2117.
[21] F. Tancret, J. Mater. Sci. Lett. 19 (2000) 1557–1558.
[22] H.F. Fischmeister, E. Arzt, Powder Metall. 26 (1983) 82–88.
[23] E. Arzt, Acta Metall. 30 (1982) 1883–1890.
[24] S.K. Maiti, M.F. Ashby, L.J. Gibson, Scr. Metall. 18 (1984) 213–217.
[25] V.V. Skorokhod, Rheological Basis of Theory of Sintering, Naukova Dumka, Kiev, 1972.
[26] A.S. Helle, K.E. Easterling, M.F. Ashby, Acta Metall. 33 (1985) 2163–2174.
[27] R.M. German, Sintering Theory and Practice, John Wiley & Sons, Inc., New York, NY, 1996.
[28] R.M. German, Particle Packing Characteristics, Industries Federation, Princeton, NJ, 1989.
[29] C.J. Li, R.M. German, Metall. Mater. Trans. 14A (1983) 2031–2041.
[30] A. Belhadjhamida, R.M. German, Tungsten and Tungsten Alloys by Powder Metallurgy—A Status Review, Tungsten and Tungsten Alloys, TMS, Pennsylvania, 1991.
[31] C.L. Briant, B.P. Bewlay, MRS Bull. (1995) 67–73.
[32] S.W.H. Yih, C.T. Wang, Tungsten, Plenum Press, New York, 1979.
[33] R.M. German, Z.A. Munir, Metall. Mater. Trans. 7A (1976) 1873–1877.
[34] H.W. Hayden, J.H. Brophy, J. Electrochem. Soc. 110 (1963) 805–810.
[35] L.L. Seigle, C.D. Dickinson, Refractory Metals and Alloys, vol. 17, Interscience Publishers, New York, NY, 1963.
[36] I.H. Moon, J.Y. Kim, Y.D. Kim, Int. J. Refract. Met. Hard Mater. 3 (1984) 176–179.
[37] J.C. Knight, A.S. Wagh, W.A. Reid, J. Mater. Sci. 21 (1986) 2179–2184.
[38] S.C. Danforth, M.H. Richman, Am. Ceram. Soc. Bull. 62 (1983) 501–504.